Giant, 17, 2024, 100205

Full-length article

Topological effect on mechanical properties of self-assembled block copolymer

Suhail K. Siddique[a], Hassan Sadek[a], Tsung-Lun Lee[a], Gkreti-Maria Manesi[b], Apostolos Avgeropoulos[b], Chi-Wei Wang[c], Chang-Chun Lee[c], Edwin L. Thomas[d], Rong-Ming Ho[a,*]

[a] Department of Chemical Engineering, National Tsing Hua University, Hsinchu 30013, Taiwan
[b] Department of Materials Science Engineering, University of Ioannina, University Campus, Ioannina 45110, Greece
[c] Department of Power Mechanical Engineering, National Tsing Hua University, Hsinchu 30013, Taiwan
[d] Department of Material Science and Nanoengineering, Texas A&M University, College Station, Texas, United States

Keywords: Block copolymer, Self-assembly, Topology effect, Thin film, Nanoindentation, Reduced elastic modulus

Herein, this work aims to demonstrate the topological effect on the mechanicalx characteristics of self-assembled block copolymers (BCPs). The lamellae-forming polystyrene-*block*-polydimethylsiloxane (PS-*b*-PDMS) can be self-assembled into various nanostructured monoliths with the use of PS-selective solvent for solvent annealing, giving diamond, gyroid, and cylinder structures with increasing the swelling degree of PS domain (the effective volume fraction of the PS segment after solvent annealing followed by evaporation). The stiffness of the self-assembled monoliths is scrutinized by nanoindentation test. For intrinsic PS-*b*-PDMS monolith with lamellar structure, the reduced elastic modulus as calculated from the measured stiffness is 0.91 GPa. By contrast, the PS-*b*-PDMS monolith with cylinder structure gives a significant reduction in reduced elastic modulus with the value of 0.52 GPa due to the introduced microporosity to the PS domain from solvent annealing using PS-selective solvent, resulting in the lower confrontation for continuous layer-by-layer deformation of hard PS and soft PDMS domains. In the case of gyroid-structured PS-*b*-PDMS monolith, it is unexpected to exhibit a significant increase in the reduced elastic modulus with a value of 1.6 GPa: note that the effect of microporosity is still significant. Accordingly, the enhancement of the reduced elastic modulus is attributed to the effect of deliberate structuring with network topology (***i.e.,*** three-dimensional co-continuous hard PS and soft PDMS domains) that is able to hold the occurrence of large-scale deformation. In contrast to the gyroid with a three-strut texture, the diamond-structured PS-*b*-PDMS monolith with a four-strut texture is superior to the gyroid with a reduced elastic modulus of 2.2 GPa, further confirming the suggested topology effect.

* Corresponding author.
E-mail address: rmho@mx.nthu.edu.tw (R.-M. Ho).
Received 21 May 2023; Received in revised form 6 October 2023; Accepted 30 October 2023

https://doi.org/10.1016/j.giant.2023.100205

1 Introduction

Mechanical properties of materials have been one of the most widely studied areas in material science for exploring various applications in our daily life. Numerous efforts have been devoted to improve the mechanical properties of materials by hybridization to tune the constituent compositions and corresponding microstructures [1]. Nature has shown the finest approach for the fabrication of mechanically superior materials by incorporating an interpenetrated structure with hard and soft material segments [2]. Natural systems like nacre [3], stomatopod dactyl club [4], and woods [5] show composite structures or assemblies of multiple elements fashioned for superior mechanical properties. Note that interpenetrating phase composites are materials that are composed of two or more phases with topologically continuous and three-dimensional interconnected structures, giving a substantially enhanced mechanical performance [6–8].

This pursuit implies that the mechanical properties of the materials can be controlled by the constituent composition and the structure of the material. Natural and synthetic interpenetrating phase composites have drawn intensive attention for practical applications due to their exceptional mechanical properties such as high modulus and strength as well as superior toughness [9–11]. A large part of the study of material science is devoted to fabricate mechanically superior composites with network texture; this pursuit from its earliest origin has involved the manipulations of large and small material features by a top-down approach [12,13]. However, fabrication of well-ordered structures by the top-down methods might not be cost-effective and the architectural features have constraints to go below 100 nm size. By contrast, the fabrication process by a bottom-up approach may provide an easy fabrication technique and a smaller feature size. The bottom-up methods refer to the building of materials through the self-assembly of an atom-by-atom, and molecule-by-molecule [14]. Block copolymers (BCPs) have been extensively studied due to their ability to self-assemble into a variety of nanostructures. Owing to the incompatibility of distinct blocks, block copolymers (BCPs) can be self-assembled into lamella, gyroid, diamond, cylinder, and spheres with readily adjustable sizes, depending on their constituent composition [15–17]. Double gyroid (DG) and double diamond (DD) phases were discovered in BCPs showing prominent positions in the architectural arena due to their unique network structure [18]. The DG phase consists of two interpenetrated trigonal planar geometry with three arms in which each arm connects to another to form a 3D network whereas the DD phase consists of tetrahedral geometry with four interconnected networks from four arms. The superior mechanical behavior of the DG phase due to their unique network geometry as compared to the classical morphologies was first discovered by Thomas et al. [19,20]. Recently, the enhanced energy dissipation from the deliberate structuring of nanonetwork textures for thermosets fabricated by templated polymerization has been demonstrated by Ho et al. by enabling the design of mechanical metamaterials from a bottom-up approach [21,22]. In fact, the mechanical properties can be enhanced by increasing the strut numbers of the nanonetworks from gyroid to diamond [23,24]. However, systematic comparison of mechanical properties with topological effect, in particular from network structure on the BCP performance is minimally touched.

Herein, this work aims to demonstrate the mechanical properties of nanostructured monoliths fabricated by controlled self-assembly through solvent annealing of stable lamellae-forming polystyrene-*block*-polydimethylsiloxane (PS-*b*-PDMS) with distinct geometries (Fig. 1). Owing to the large interaction parameter of PS-*b*-PDMS, it is feasible to acquire a variety of nanostructured monoliths including cylinder (C), lamellae (L), double gyroid (DG), and double diamond (DD) from the same PS-*b*-PDMS with invariant weight fractions of constituted blocks by tuning the effective volume fraction of the PS with the use of PS-selective solvent (Chloroform) for solvent annealing through the control of nitrogen-purge flow rate.

2 Experimental section

2.1 Materials

A stable lamellae-forming PS-*b*-PDMS with the volume fraction of PDMS $f_{PDMS}{}^{v}$ = 0.41 ($M_n{}^{PS}$= 51,000 g/mole, $M_n{}^{PDMS}$= 35,000 g/mole, $Đ_M$ = 1.05) was used in this study. The detailed synthesis of the PS-*b*-PDMS was discussed in our previous publications [25–27].

2.2 PS-b-PDMS monolyth fabricated by dip coating

To generate uniform films over a large area [28] for mechanical property test, PS-*b*-PDMS monoliths were prepared by dip coating on a silicon wafer with controlled thickness; after casting, a uniform film with disordered nanonetwork texture can be formed, indicating that the microphase separation can occur even with fast solvent evaporation due to the large interaction parameter of the silicon-containing block copolymer. Consequently, solvent annealing in a solvent annealing chamber using chloroform as a selective solvent was conducted to improve the degree of order by increasing the chain mobility of BCP chains for self-assembly. By taking advantage of the solvent flow rate and annealing time, it is feasible to obtain various nanostructures using the same BCP monoliths. Subsequently, PS-*b*-PDMS monoliths with different effective PS volume fractions and the same weight fraction can be fabricated [29].

2.3 Nanoindentation measurements

The Hysitron Ti950 triboindenter (Hysitron Inc.) was used to perform nanoindentation tests using a spherical indenter. The indentation measurements were conducted on a film sample with a 5 μm thickness silicon substrate at room temperature. The load-displacement curve was recorded at the same rate of loading and unloading (60 μN/sec) with a maximum load of 1000 μN. In the nanoindentation tests, the load-displacement data were recorded continuously while the tip was driven into the PS-*b*-PDMS thin film. The reduced elastic modulus can be calculated from the load-displacement curve (P-h) based on the Oliver-Pharr model. In each unloading curve, the elastic modulus can be calculated to get a consistent result.

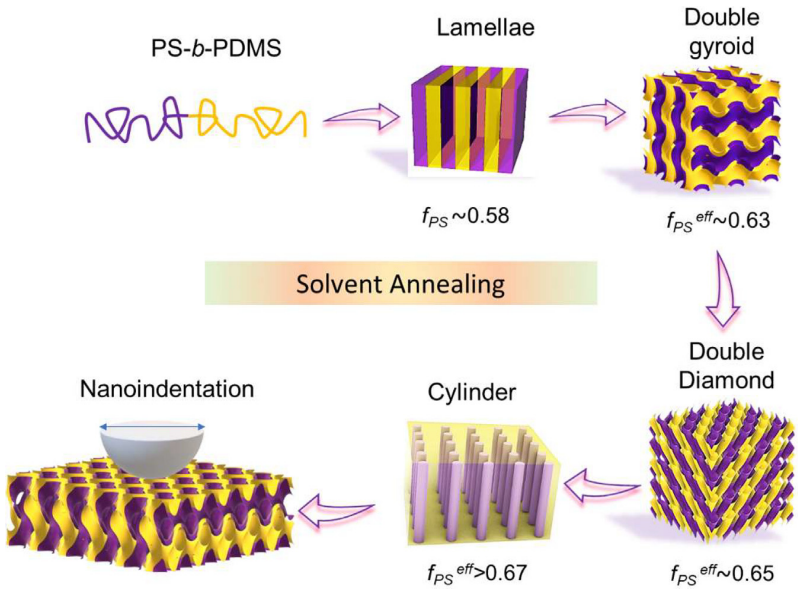

Fig. 1

Schematic illustration of the showcase for the mechanical property analysis of self-assembled morphologies including lamellae, double gyroid, double diamond, and cylinder structures from the controlled self-assembly of lamellae forming PS-*b*-PDMS by nanoindentation test with spherical indenter having a nominal radius of 0.5–1.5 μm.

In the present study, the reduced elastic modulus E_r was determined from the P-h curve, using the Sneddon formula.

$$E_r = \frac{\sqrt{\pi}}{2}\frac{S}{\sqrt{A_t}}$$

Here, E_r is the reduced elastic modulus (indentation modulus) which represents the elastic deformation that occurs in the sample and the indenter. S and A_t represent the stiffness and the projected contact area, respectively. Note that the deformation in the diamond indenter tip is negligible. Moreover, the elastic and plastic response also can be observed through a load-displacement curve. As a result, the reduced elastic modulus (indentation modulus) is a representative value for discussion on mechanical performance.

3 Results and discussion

A simple diblock copolymer system of PS-*b*-PDMS with PDMS volume fraction (f_{PDMS}^{v}) of 0.41 was used in this study. The detailed synthesis procedure was explained in our previous publication [25]; Table S1 shows the detailed information for the PS-*b*-PDMS used in this study. By taking advantage of the intrinsic large interaction parameter of silicon-containing BCP, the self-assembled morphology is strongly dependent on the solvent used for solvent annealing. Accordingly, the BCP thin film was fabricated by dip coating, and PS-*b*-PDMS monolith can be self-assembled into stable layer-by-layer lamellae phase with PS volume fraction (f_{PS}^{v}) of 0.58 by thermal annealing at 180 °C for 24 h as shown in Fig. 2a. Considering the narrow window for the formation of network phases, it is feasible to acquire triply periodic phases by using a PS-selective solvent chloroform for a morphological transition from the thermodynamically stable lamellar phase to nanonetwork-structured BCP monoliths in metastable condition. As shown in Fig. 2b, double gyroid-structured PS-*b*-PDMS was obtained after controlling the solvent flow rate through instantaneous purging of pure nitrogen gas to trap the forming morphology of the swollen films where the effective volume fraction for PS (f_{PS}^{eff}) is 0.63 as reported previously [29]. Subsequently, a well-ordered double diamond structure with f_{PS}^{eff}~0.65 can be obtained by further increasing the selective swelling of PS block in PS-*b*-PDMS through the increased flow rate of selective solvent (Fig. 2c). As reported previously [29], there should be no issue with the concern of structural variation along the thickness direction. As shown in Figs. S1a and S1b, the self-intermediate phase after solvent annealing at a high flow rate of 20 mL/min for 15 h and 30 h. Consequently, there is no heterogeneity in the self-assembled structures. Apparently, the maximum flow rate of selective solvent to the PS-*b*-PDMS can deliver the rod-like textured cylinder as exemplified in Fig. 2d, indicating the formation of a cylinder-structured PS-*b*-PDMS with the f_{PS}^{eff}>0.67. By taking advantage of the same weight fraction of PS and PDMS in the PS-*b*-PDMS synthesized with distinct self-assembled morphologies having different effective volume fractions of PS (f_{PS}^{eff}), the comprehensive study of the topological effect on mechanical properties can be conducted for systematic comparisons. To provide an insight into the mechanical properties of self-assembled PS-*b*-PDMS monoliths, it is necessary to understand the characteristic behaviors of intrinsic PS and PDMS. Typical nanoindentation tests with calibrated spherical intender at a loading rate of 60 μN/s were used in a cyclic mode until 1000 μN to examine the load-displacement curve for intrinsic PS. As shown in Fig. 3a, a typical load-displacement curve having multiple cyclic loading with a maximum load of 1000 μN was acquired for intrinsic PS. Owing to the robust stiffness of

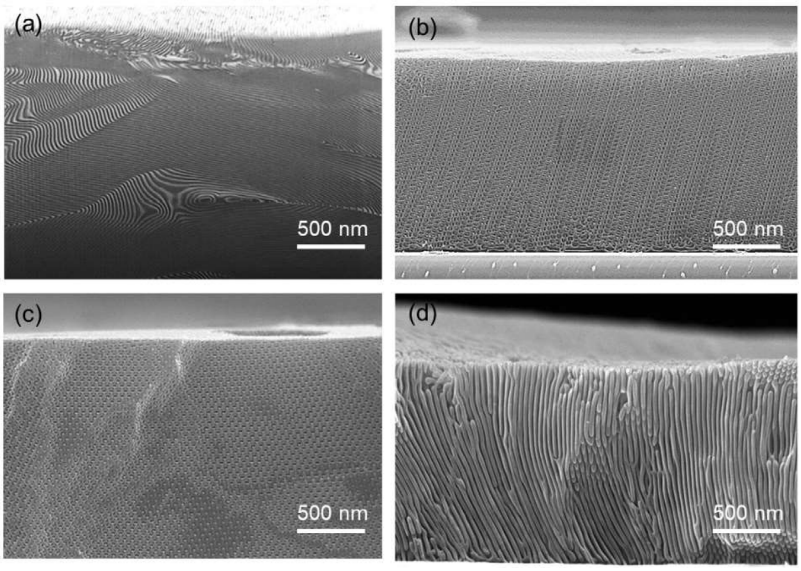

Fig. 2

FESEM micrographs of cross-sectional-view of (a) lamellae- (b) double gyroid- (c) double diamond- and (d) cylinder-structured PS-*b*-PDMS monoliths.

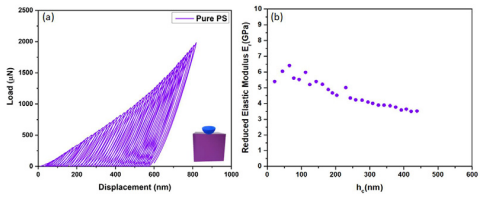

Fig. 3

(a) The load-displacement curves of intrinsic PS; (b) Reduced elastic modulus (E_r) of intrinsic PS as a function of displacement.

intrinsic PS, the maximum displacement (h_{max}) attained at a load of 1000 μN is approximately 500 nm; note that where the least displacement with considerable retraction of the unloading curve signifies the PS as a hard domain. Subsequently, the reduced elastic modulus (E_r) of intrinsic PS can be calculated from the initial slope of each unloading curve. As shown in Fig. 3b, the reduced elastic modulus of intrinsic PS was calculated as 3.4 GPa; note that the initial disparity in modulus is considered as a preliminary shift due to the asymmetry in contact between the indenter and the surface of the sample. By contrast to intrinsic PS, PDMS shows a high recovery character while unloading with a large retraction of the unloading curve as shown in Fig. S2a; the reduced elastic modulus was calculated as 0.002 GPa (Fig. S2b), referred as the soft dispersed microdomain in the self-assembled PS-*b*-PDMS. Accordingly, with a volume fraction (f_{PDMS}) of approximately 0.41 in the self-assembled block copolymer, the amalgamation of soft and hard domain interaction of self-assembled samples for mechanical anisotropy can be scrutinized.

To assess the effect of aimed topology on mechanical properties, the PS-*b*-PDMS can be self-assembled with a sequential arrangement of hard PS and soft PDMS using solvent annealing for selective swelling of PS. However, the variation of the effective volume fraction of PS attributed to the fast evaporation of PS-selective solvent leaves the PS domain with various closed microporosities, which is confirmed by the reduction in the modulus of pure PS (Fig. S3), whereas the occupied volume of PDMS remains constant. The detailed swelling behavior of block copolymer has been discussed previously.[29,30] Note that microporosity causes a reduction in the modulus of materials.

The mechanical characterization of self-assembled monoliths using nanoindentation was scrutinized to evaluate the topology effect on mechanical properties. Fig. 4a shows typical load-displacement curves for the lamellae and cylinder acquired by using nanoindentation test with cyclic loading at a maximum load of 1000 μN; note that the cyclic loading can be used to obtain a consistent result from nanoindentation.

Primarily, the lamellae-structured PS-*b*-PDMS show a large displacement (deformation) while loading. As shown in Fig. 4a, the maximum deformation in lamellae-structured monoliths is nearly reached approximately 2000 nm. Moreover, the unloading curve after withdrawing the nanoindenter shows significant retraction related to the elastic deformation of PS-*b*-PDMS monolith; which signifies that the unloading curves in lamellae-structured PS-*b*-PDMS show large elastic recovery. Note that the lamellae-structured PS-*b*-PDMS possesses the minimum effective volume fraction hard PS domain (0.58), although without any closed micropores by swelling, which relatively provides robust stiffness to the hard PS domain. However, the significant elastic recovery can be attributed to the dominating character of the continuous soft PDMS domain ($f_{PDMS}{}^{v}$ 0.42); note that the hard PS and soft PDMS domains are arranged in a layer-by-layer form. Subsequently, the collective deformations are due to the combined effect of hard PS domain without any internal microporous structure and soft PDMS layer. As a result,

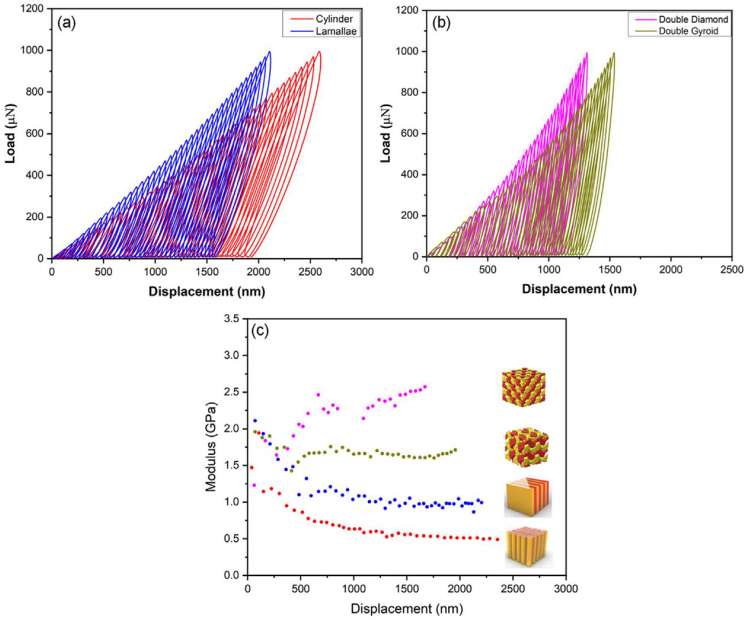

Fig. 4

(a) The load-displacement curves of cylinder- and lamellae-structured PS-*b*-PDMS monoliths; (b) The load-displacement curves of double-gyroid and double-diamond structured PS-*b*-PDMS monoliths; (c) Reduced elastic modulus of self-assembled monoliths with variety of nanostructures as a function of displacement.

the lamellae-structured PS-*b*-PDMS is expected to exhibit lower stiffness due to the layer-by-layer structure of soft PDMS domain with elastic dominance but is superior as compared to cylinder-structured PS-*b*-PDMS due to hard PS without any microporous structure due to swelling.

Moreover, the load-displacement curve for cylinder morphology shows the initial deformation starts without any tenacity toward loading which gradually leads to substantial depth under nanoindenter. By increasing the loading, the displacement could reach up to 2700 nm at a maximum load of 1000 μN which is much higher as compared to the stable lamellae-structure (2000 nm). Moreover, the cylinder-structured monolith can exhibit considerable repose while withdrawing the nanoindenter; as a result, all unloading curves show similar characteristics with nearly 25 % elastic recovery which implies the deformation character should be largely contributed by elasticity. Note that the PS-*b*-PDMS monolith having cylinder structure was attained after maximum swelling of the PS microdomain under a controlled solvent rate, where a significant change in occupied volume of PS can be occurred (f_{PS}^{eff} >0.67), which exceptionally softens the hard PS domains by intruding extensive amount of closed microporous structure as compared to as-cast lamellae structure. Furthermore, the soft PDMS domain is indeed embedded as one-dimensionally organized cylinders with the same occupied volume in the microporous PS matrix.

Owing to the synergic effect of closed micropores in hard PS matrix and one-dimensionally ordered soft PDMS, it is feasible to obtain lower stiffness for the PS-*b*-PDMS with cylinder morphology. To further investigate the topology effect on mechanical property, the PS-*b*-PDMS monolith with gyroid structure was examined using a nanoindentation test. Interestingly, as shown in Fig. 4b, the PS-*b*-PDMS with gyroid structure shows significant constraint towards deformation. In contrast to the cylinder and lamellae-structured PS-*b*-PDMS, the gyroid structure shows a maximum displacement of 1500 nm; note that the cylinder and lamellae exhibit 2700 nm and 2000 nm for the maximum displacement, respectively. Apparently, the characteristic deformation having a persistence deform in each loading thus exhibits the least depth under the nanoindentation. Surprisingly, after withdrawing the nanoindenter, each unloading curve exhibits low retraction as compared to the elastic rebound in the cylinder and lamellae. Indeed, the DG-structured PS-*b*-PDMS monolith shows the plastic mode of deformation with insignificant retraction of almost less than 5 %. This exceptional deformation character in the DG-structured monolith is attributed to the trigonal planar structure of the soft PDMS domain with interconnected three arms as a network texture in the hard PS matrix. The effective volume fraction of the hard PS domain (0.63) in DG-structured PS-*b*-PDMS was smaller than the cylinder (>0.67) and larger than the lamellae-structured PS-*b*-PDMS (0.52); note that the effect of microporosity is still significant.

Accordingly, the exceptional deformation mechanism can be contributed by co-continuous structure as compared to the ones with cylinder and lamellar texture. This inferred that the deliberate structure with three-dimensional soft PDMS networks in the hard PS matrix should contribute to the deformation character dominated by the PS matrix even with the microporosity. As a result, the hard PS domain can be able to guard against large deformation while loading due to a supportive interconnected network between the PS matrix with a trigonal planar structure. Apparently, the tenacity of DG-structured PS-*b*-PDMS towards deformation is attributed to the

topology effect from the deliberate structuring with such co-continuous texture instead of microporosity due to swelling, which provides exceptional mechanical properties (*i.e.*, the corresponding modulus and stiffness as well).

To further explore the effect of deliberate structuring for the interpenetrated network texture on mechanical properties, a diamond-structured monolith was also fabricated for the nanoindentation test. Consistently, the diamond-structured PS-*b*-PDMS shows superior tenacity towards deformation as compared to the one with cylinder and lamellae. As shown in Fig. 4b, the spherical nanoindenter needs to exert a large load to deform the diamond structure under each load at which the maximum deformation can reach only 1350 nm at a maximum load of 1000 μN. Similar to the load-displacement curves of trigonal planar (DG-structured) PS-*b*-PDMS, the collective load-displacement curve exhibits a concave pattern to establish the considerable stiffness of the monolith with the diamond structure. Note that the diamond-structured PS-*b*-PDMS possesses PS effective volume fraction of f_{PS}^{eff} ~0.65 at which the PS hard domain might have considerable micropores due to swelling. However, in contrast to gyroid-structured PS-*b*-PDMS monolith, the diamond structure has an additional ligament (four struts) connected throughout the PS hard matrix which can further support the hard domain to withstand the applied loading [21]. Furthermore, the diamond-structured PS-*b*-PDMS monolith gives a comparable unloading pattern with the plastic mode of deformation without considerable retraction, which indicates that the tree-dimensionally ordered soft PDMS domains with an additional number of struts can be able to dissipate the energy through the struts can restrict the elastic mode of deformation.

As a result, the reduced elastic modulus of self-assembled monoliths was calculated from each load-displacement curve (P-h) by the Oliver Pharr model [31]. As shown in Fig. 4c, the thermodynamically stable lamellae structured PS-*b*-PDMS shows the reduced elastic modulus with a value of 0.91 GPa; note that there is no effect of microporosity due to swelling. In contrast to the two-dimensionally ordered layer-by-layer structure of lamellae with alternating soft PDMS and hard PS, the hexagonally packed cylinder-structured PS-*b*-PDMS with a significant effect of microporosity shows the least reduced elastic modulus with a value of 0.52 GPa. Interestingly, the gyroid-structured PS-*b*-PDMS shows a significant increase in the reduced elastic modulus; as shown in Fig. 4c, the reduced elastic modulus of the gyroid-structured monolith was calculated as 1.6 GPa, which is three times the elastic modulus of cylinder structure and considerably higher as compared to lamellae-structured (0.91 GPa) PS-*b*-PDMS monoliths. This exceptional increase in reduced elastic modulus of the gyroid-structured monolith as compared to the cylinder and lamellae is indeed attributed to the trigonal planar interconnected structure embedded in the PS matrix with co-continuous texture at which the two PDMS networks interpenetrate throughout space within a matrix of continuous hard PS. Apparently, the presence of the glassy hard PS can show moderate swelling with solvent annealing; however, the interconnected network phase plays a vital role in reducing the rapid deformation to enhance the stiffness while loading. Furthermore, an interconnected three arms of a trigonal planar-

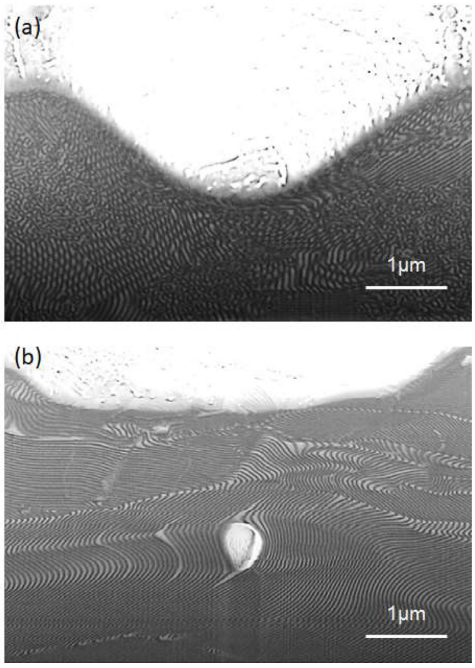

Fig. 5

Cross-sectional FESEM micrograph of (a) cylinder-structured and (b) lamellae-structured PS-*b*-PDMS after nanoindentation using spherical indenter with a nominal radius of 0.5–1.5 μm.

structured soft PDMS domain can dissipate the applied stress, which further restricts the elastic rebound while unloading. Note that the absolute value for the reduced elastic modulus was determined based on the consistent values as a function of the displacement. To establish the suggested topology effect, the diamond-structured PS-*b*-PDMS monolith consistently gives rise to a similar fashion under loading. Most interestingly, the reduced elastic modulus for diamond-structured PS-*b*-PDMS monolith shows an exceptionally high value of 2.2 GPa. Considering the narrow window of volume fraction for the formation of gyroid and diamond structure, the selective swelling of PS by solvent should be nearly the same with slightly enhanced swelling on the diamond-structured monolith. However, the difference in reduced elastic modulus is indeed considerably high in the case of diamond structure as compared to the gyroid-structured monolith (1.6 GPa). This remarkable enhancement in reduced elastic modulus is attributed to the tetrahedral morphology with four arms connected. Accordingly, the four arms of soft PDMS domains interconnected to each other can provide successive space for hard PS to connect with additional strut support in three-dimensional. Furthermore, interconnected soft PDMS domains can dissipate the applied stress through the four-armed structure which restricts elastic recovery. As a result, with the effect of deliberate structuring with network texture as well as the number of connective arms for networking, the reduced elastic modulus can be enhanced, and the deformation will become smaller.

To further examine the suggested deformation behavior, a cross-sectional FESEM image was used to investigate the residual indented locations (Fig. S4). As shown in Fig. 5a, the PS-*b*-PDMS

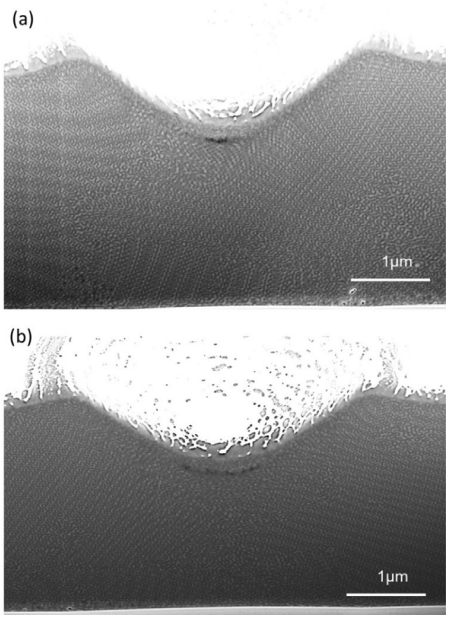

Fig. 6

(a) Cross-sectional FESEM micrographs of (a) DG-structured (d) DD-structured PS-*b*-PDMS after nanoindentation using spherical indenter with a nominal radius of 0.5–1.5 μm.

with hexagonally packed cylinder morphology will experience significant depth under loading; at which the hard PS domain with a large amount of microporosity cannot act as a support to withstand the applied force due to approximately 9 % of intruding microporosity; note that the soft PDMS domains arranged in one-dimensionally organized individual rods-like textures. Moreover, the cross-sectional FESEM shows cylinder morphology exhibits no preferred orientations, which might also be attributed to the least tenacity towards deformation. Moreover, the two-dimensionally continuous lamellae-structured PS-*b*-PDMS shows alternative soft PDMS domain and hard PS domain stalked together; under compression, the deformation happens simultaneously in both phases (Fig. 5b). The effective large deformation of the soft PDMS layer can be constrained by the hard PS layer; note that there is the effect of microporosity. As a result, the soft and hard microdomains can deform cooperatively or simultaneously with appropriate hard and soft segment support to provide elastic deformation and a higher effective reduced modulus as compared to cylinder morphology. Owing to the plastic deformation for the soft and hard microdomains, it is reasonable to expect that an isotropic gyroid- and diamond-structure soft PDMS domain interpenetrating within the hard PS matrix with trigonal planar and tetrahedral textures can effectively restrict the rapid deformation, resulting in less deformation under loading. As shown in Fig. 6a, for gyroid-structured PS-*b*-PDMS, the interpenetrated PDMS soft domain would be connected from one trifunctional node to another throughout the hard PS matrix. While under compression, the initial deformation needs to happen on the top layer of the triply periodic gyroid layer. Owing to the higher stiffness, it is necessary to apply a large force to deform the bottom layers. Accordingly, the intermediate network phase can disturb the continuous deformation of PS. Subsequently, the gyroid can show deformation of each gyroid unit cell leading to the least deformation (Fig. 4a). In the case of a diamond, the tetrahedral morphology has an additional connection toward the node that can further reduce the degree of deformation as compared to DG phase. As shown in Fig. 6b, four PDMS ligaments diamond structures are connected to the nodes building up significant network areas in the PS matrix. Indeed, the hard PS domain immersed between the network structure dominates the effect of the hard PS domain. Consequently, extra strut support can be occurred for diamond structure as compared to gyroid; note that similar deformation behaviors can be both recognized in the gyroid- and diamond-structured BCPs. As a result, the initial reduced elastic modulus of an isotropic polygranular gyroid and diamond samples shows mechanically robust characteristics than the classical morphologies; namely, it requires higher stresses for the initiation of the deformation, giving higher stiffness than the one-dimensional cylinder and two-dimensional lamellae even with the existent porosity for the PS matrix. The nanoindentation results suggest the anisotropic effect on mechanical properties due to the topology of the self-assembled block copolymer. To reaffirm the effect of deliberate structure on mechanical deformation of DG and DD structures of self-assembled morphologies under equivalent stress, linear elastic calculations of vertically contracted nanonetwork models under nanoindentation were conducted by finite element analysis (FEA); an equivalent plastic deformation zone of the monoliths was calculated under normalized solid bulk with equivalent stress, especially in the post-yield deformation. As shown in Fig. 7a, the

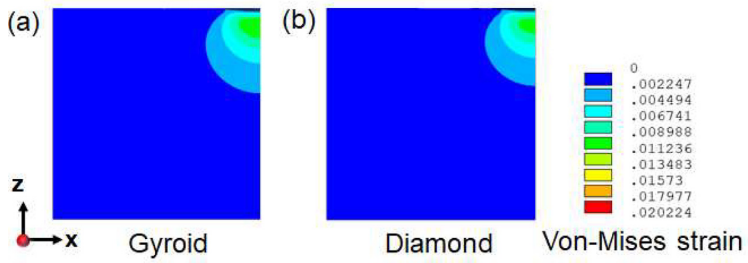

Fig. 7

Calculated plastic deformation zone for (a) gyroid and (b) diamond by finite element analysis.

gyroid-structured PS-*b*-PDMS exhibits a slightly large deformation capability as compared to the diamond-structured PS-*b*-PDMS (Fig. 7a), which reassures the least tenacity of diamond structure towards deformation as compared to gyroid. Note that the four-fold symmetry of diamond-structured PS-*b*-PDMS greatly increases the reduced elastic modulus due to tetrahedral structure. As a result, the tetrahedral diamond structure restricts the large strain which leads to enhanced stiffness to DD as compared to DG. Furthermore, owing to the synergic effect of deliberate structure and four-fold symmetry, the diamond one shows significant support against the deformation which reassures the results from nanoindentation.

4 Conclusion

In summary, PS-*b*-PDMS can be self-assembled into a variety of nanostructures including cylinders, lamellae, gyroid, and diamond by solvent annealing using PS selective solvent with invariant weight fractions and different effective volume fractions of hard PS. The equilibrium morphology of lamellae-structured PS-*b*-PDMS shows moderately reduced elastic modulus due to the layer-by-layer structure of hard PS and soft PDMS. However, the cylinder-structured PS-*b*-PDMS monoliths exhibit the least reduced elastic modulus due to the significant amount of micropores to soften the hard PS domain by extensive swelling by selective solvent. Moreover, the gyroid and diamond structured PS-*b*-PDMS show significant enhancement of reduced elastic modulus due to the well-ordered interconnected hard PS matrix that could restrict the rapid deformation due to the interpenetrated network structure. With an additional PDMS strut in the diamond structure (tetrahedral texture), the gyroid can significantly enhance the reduced elastic modulus due to the number of ligaments, reflecting the topological effect of self-assembled BCPs on mechanical performance.

Declaration of Competing Interest

The authors declare that they have no known competing financial interests or personal relationships that could have appeared to influence the work reported in this paper.

Data availability

Data will be made available on request.

Acknowledgment

We thank the Ministry of Science and Technology of the Republic of China, Taiwan, for financially supporting this research under MOST 110-2124-M-007-001 and MOST 110-2221-E-007-004-MY3. We also thank The National Synchrotron Radiation Research Center (NSRRC, Taiwan) for its assistance in the Synchrotron SAXS experiments. The research work was partially supported by the Bodossaki Foundation, under the "Stamatis G. Mantzavinos" Memorial Postdoctoral Scholarships Programme for G. M. Manesi (BDA-7255). We thank the National Science Foundation DMR for supporting this research work under award DMR 2105296.

Supplementary materials

Supplementary material associated with this article can be found, in the online version, at doi:10.1016/j.giant.2023.100205.

References

[1] L.J. Gibson, M.F. Ashby, Cellular Solids: Structure and Properties, 2 ed., Cambridge University Press, Cambridge, 1997.

[2] W. Huang, M. Shishehbor, N. Guarín-Zapata, N.D. Kirchhofer, J. Li, L. Cruz, T. Wang, S. Bhowmick, D. Stauffer, P. Manimunda, K.N. Bozhilov, R. Caldwell, P. Zavattieri, D. Kisailus, A natural impact-resistant bicontinuous composite nanoparticle coating, Nat. Mater. 19 (11) (2020) 1236–1243.

[3] J. Wang, Q. Cheng, Z. Tang, Layered nanocomposites inspired by the structure and mechanical properties of nacre, Chem. Soc. Rev. 41 (3) (2012) 1111–1129.

[4] J.C. Weaver, G.W. Milliron, A. Miserez, K. Evans-Lutterodt, S. Herrera, I. Gallana, W.J. Mershon, B. Swanson, P. Zavattieri, E. DiMasi, D. Kisailus, The stomatopod dactyl club: a formidable damage-tolerant biological hammer, Science 336 (6086) (2012) 1275–1280.

[5] U.G.K. Wegst, H. Bai, E. Saiz, A.P. Tomsia, R.O. Ritchie, Bioinspired structural materials, Nat. Mater. 14 (1) (2015) 23–36.

[6] M. Frey, L. Schneider, K. Masania, T. Keplinger, I. Burgert, Delignified wood–polymer interpenetrating composites exceeding the rule of mixtures, ACS Appl. Mater. Interface. 11 (38) (2019) 35305–35311.

[7] C. Ahn, S.-M. Kim, J.-W. Jung, J. Park, T. Kim, S.E. Lee, D. Jang, J.-W. Hong, S.M. Han, S. Jeon, Multifunctional polymer nanocomposites reinforced by 3D continuous ceramic nanofillers, ACS Nano 12 (9) (2018) 9126–9133.

[8] J. Bauer, M. Sala-Casanovas, M. Amiri, L. Valdevit, Nanoarchitected metal/ceramic interpenetrating phase composites, Sci. Adv. 8 (33) (2022) eabo3080.

[9] L. Wang, J. Lau, E.L. Thomas, M.C. Boyce, Co-continuous composite materials for stiffness, strength, and energy dissipation, Adv. Mater. 23 (13) (2011) 1524–1529.

[10] J. Kim, Y. Cho, S. Kim, J. Lee, 3D cocontinuous composites of hydrophilic and hydrophobic soft materials: high modulus and fast actuation time, ACS Macro Lett. 6 (10) (2017) 1119–1123.

[11] J.-H. Lee, L. Wang, M.C. Boyce, E.L. Thomas, Periodic bicontinuous composites for high specific energy absorption, Nano Lett. 12 (8) (2012) 4392–4396.

[12] N. Bhandaru, S. Roy, G. Harikrishnan, R. Mukherjee, Lithographic tuning of polymeric thin film surfaces by stress relaxation, ACS Macro Lett. 2 (3) (2013) 195–200.

[13] A. Schwab, R. Levato, M. D'Este, S. Piluso, D. Eglin, J. Malda, Printability and shape fidelity of bioinks in 3D bioprinting, Chem. Rev. 120 (19) (2020) 11028–11055.

[14] G.M. Whitesides, B. Grzybowski, Self-assembly at all scales, Science 295 (5564) (2002) 2418–2421.

[15] F.S. Bates, G.H. Fredrickson, Block copolymer thermodynamics: theory and experiment, Annu. Rev. Phys. Chem. 41 (1) (1990) 525–557.

[16] F.S. Bates, Polymer-polymer phase behavior, Science 251 (4996) (1991) 898–905.

[17] F.S. Bates, G.H. Fredrickson, Block copolymers-designer soft materials, Phys. Today (2000) 52.

[18] E.L. Thomas, D.B. Alward, D.J. Kinning, D.C. Martin, D.L. Handlin, L.J. Fetters, Ordered bicontinuous double-diamond structure of star block copolymers: a new equilibrium microdomain morphology, Macromolecules 19 (8) (1986) 2197–2202.

[19] B.J. Dair, C.C. Honeker, D.B. Alward, A. Avgeropoulos, N. Hadjichristidis, L.J. Fetters, M. Capel, E.L. Thomas, Mechanical properties and deformation behavior of the double gyroid phase in unoriented thermoplastic elastomers, Macromolecules 32 (24) (1999) 8145–8152.

[20] B.J. Dair, A. Avgeropoulos, N. Hadjichristidis, E.L. Thomas, Mechanical properties of the double gyroid phase in oriented thermoplastic elastomers, J. Mater. Sci. 35 (20) (2000) 5207–5213.

[21] S.K. Siddique, T.-C. Lin, C.-Y. Chang, Y.-H. Chang, C.-C. Lee, S.-Y. Chang, P.-C. Tsai, Y.-R. Jeng, E.L. Thomas, R.-M. Ho, Nanonetwork thermosets from templated polymerization for enhanced energy dissipation, Nano Lett. 21 (8) (2021) 3355–3363.

[22] K.-C. Yang, P. Puneet, P.-T. Chiu, R.-M. Ho, Well-Ordered nanonetwork metamaterials from block copolymer templated syntheses, Acc. Chem. Res. 55 (15) (2022) 2033–2042.

[23] S.K. Siddique, H. Sadek, C.-W. Wang, C.-C. Lee, C.-Y. Tsai, S.-Y. Chang, C.-L. Li, C.-H. Hsueh, R.-M. Ho, Diamond-structured nanonetwork gold as mechanical metamaterials from bottom-up approach, NPG Asia Mater. 15 (1) (2023) 36.

[24] H. Sadek, S.K. Siddique, C.-W. Wang, P.-T. Chiu, C.-C. Lee, R.-M. Ho, Starfish-inspired diamond-structured calcite single crystals from a bottom-up approach as mechanical metamaterials, ACS Nano 17 (16) (2023) 15678–15686.

[25] P. Georgopanos, T.-Y. Lo, R.-M. Ho, A. Avgeropoulos, Synthesis, molecular characterization and self-assembly of (PS-b-PDMS)n type linear (n = 1, 2) and star (n = 3, 4) block copolymers, Polym. Chem. 8 (5) (2017) 843–850.

[26] C.-Y. Chang, G.-M. Manesi, C.-Y. Yang, Y.-C. Hung, K.-C. Yang, P.-T. Chiu, A. Avgeropoulos, R.-M. Ho, Mesoscale networks and corresponding transitions from self-assembly of block copolymers, Proc. Natl Acad. Sci. 118 (11) (2021) e2022275118.

[27] T.-Y. Lo, R.-M. Ho, P. Georgopanos, A. Avgeropoulos, T. Hashimoto, Direct visualization of order–order transitions in silicon-containing block copolymers by electron tomography, ACS Macro Lett. 2 (3) (2013) 190–194.

[28] T. Wen, B. Ni, Y. Liu, W. Zhang, Z.-H. Guo, Y.-C. Lee, R.-M. Ho, S.Z.D. Cheng, Towards achieving a large-area and defect-free nano-line pattern via controlled self-assembly by sequential annealing, Giant 8 (2021) 100078.

[29] T.-L. Lee, J.-W. Lin, R.-M. Ho, Controlled self-assembly of polystyrene-block-polydimethylsiloxane for fabrication of nanonetwork silica monoliths, ACS Appl. Mater. Interface. 14 (48) (2022) 54194–54202.

[30] W. Ogieglo, B. Ghanem, X. Ma, I. Pinnau, M. Wessling, How much do ultrathin polymers with intrinsic microporosity swell in liquids? J. Phys. Chem. B 120 (39) (2016) 10403–10410.

[31] W.C. Oliver, G.M. Pharr, An improved technique for determining hardness and elastic modulus using load and displacement sensing indentation experiments, J. Mater. Res. 7 (6) (1992) 1564–1583.